Interpreting the Catalytic Voltammetry of Electroactive Enzymes Adsorbed on Electrodes

Hendrik A. Heering, Judy Hirst, and Fraser A. Armstrong*

Department of Chemistry, Oxford University, Oxford OX1 3QR, England

Received: February 5, 1998; In Final Form: June 2, 1998

Steady-state electrocatalytic waveforms displayed by redox enzymes adsorbed on electrodes are analyzed to reveal and quantify important mechanistic characteristics of the active sites involved in catalysis and to elucidate the contributions of different factors in determining the overall electron-transport rates. The shape, height, steepness, and potential of the voltammetric waves are functions of mass transport, interfacial electron-transfer rates, and the intrinsic kinetic and thermodynamic properties of the enzyme. A model is constructed first for the most simple realistic case, an enzyme containing a single two-electron active site, and then this is extended to include additional electron-transfer centers that serve as intramolecular relays. Equations are derived that predict the steady-state behavior expected for different conditions, and the models are used to assess recent experimental results. An alternative perspective on enzyme catalytic electron-transport is thus presented, in which kinetics and energetics are viewed and analyzed in the potential domain.

Introduction

Electron-transport enzymes typically catalyze two-electron substrate transformations at an active site (such as a flavin), which may be served by one-electron donors or acceptors. In addressing the factors that determine the rates and organization of catalytic electron flow through such systems, we can identify properties—crucial to biological performance—that represent interesting and challenging problems in physical chemistry. For example, inequality between the reduction potentials of the substrate and of the enzyme will produce a catalytic bias so that the enzyme is tuned to favor catalysis in one particular direction.[1] The active site may or may not stabilize a one-electron state (radical). The donors/acceptors may be external—simple electron-carrier proteins—or they may be incorporated within the protein to provide a relay system (a "wire") to overcome the problem of long-range electron transfer.[2,3] The overall mechanism may therefore embody a complex interplay of events and components, and it is highly desirable to have available a technique in which active sites and their participation in catalysis are revealed in an alternative domain to those of time or concentration, the conventional variables of kinetic studies. Such a domain is the electrochemical potential; this is explored by using protein film voltammetry.

The point of protein film voltammetry is that a redox-active protein, adsorbed on an electrode surface, is interrogated electrochemically to build up a detailed picture of its chemistry. Several factors make the method a very attractive proposition for studying and elucidating the mechanisms of electron-transport enzymes:[4] the absence of complications from protein diffusion, the minuscule quantity of sample required and consequent sensitivity to trace levels of agents in the contacting electrolyte, the ability to impose rapid and precise potential control over all redox centers across a wide potential range, the direct relationship between current and catalytic rate, and of course the interactive nature of the experiment (reactions are simultaneously driven and detected). In favorable cases it is possible to observe, in the absence of substrate, voltammetric signals that arise from reversible redox transitions of active sites in the protein (nonturnover signals) and consequently, upon introducing substrate, to determine how each of these signals is transformed and amplified into catalytic waves. The areas of the nonturnover signals equate to the charges passed and hence yield the surface coverage of electroactive enzyme molecules. Analysis is further aided if the catalytic response is "binary" i.e., adsorbed enzyme molecules are either fully active or completely inactive, so that partially disabled or misoriented fractions do not contribute to the catalytic waveform. As depicted in Figure 1, catalytic electron transport by an adsorbed enzyme can be considered to involve three stages, substrate mass transport, enzyme kinetics, and interfacial electron exchange.[5] Provided interfacial electron exchange and mass transport are not limiting, the current response is controlled by the enzyme and we can acquire a detailed and quantitative description of the processes occurring.

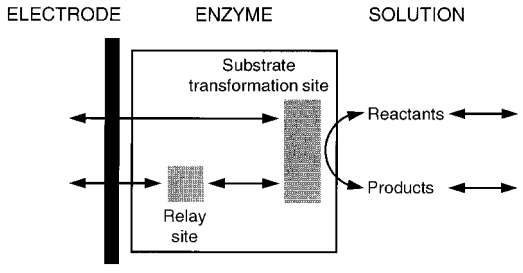

Figure 1. Schematic representation of the electron flow from an electrode to substrate, catalyzed by an adsorbed redox enzyme.

In view of these opportunities to gain fresh insight into how complex enzymes work, this paper addresses the extraction of mechanistic information from the analysis of steady-state catalytic waves. Although several models of voltammetric responses for the reduction of substrate by a monolayer of catalyst have been described,[6,7] none combine the intimate details of how catalysis occurs at an active site with both convection−diffusion of substrate and long-range electron-transfer kinetics, the two most relevant additional factors in

* Corresponding author: Inorganic Chemistry Laboratory, South Parks Road, Oxford OX1 3QR, England.

S1089-5647(98)01023-2 CCC: $15.00
Published on Web 08/12/1998

enzyme film voltammetry. With the aim of predicting complete waveforms for a variety of different situations, we have now formulated models that include both interfacial electron transfer and controlled mass transport and take into consideration the interdependence of these processes.[5−7] We have drawn comparisons with experimental data obtained for enzymes currently under investigation in our laboratory. A number of interesting results are obtained and a foundation is established for further development.

The main assumptions are that the enzyme is adsorbed as a mono/submonolayer film (but no greater coverage) of catalytically active molecules, that these molecules behave independently of each other, and that the film is homogeneous with regard to electrochemical and catalytic properties. These assumptions can be qualified to the greatest extent if nonturnover signals can be observed with sufficient clarity to be analyzed. Monolayer coverage for an enzyme of molecular weight 50 000 will typically be a few picomoles/per square centimeter; consequently, redox sites that are uniform within the film and have good electronic coupling with the electrode will give clearly visible signals, particularly if a cooperative two-electron center such as a flavin is present (since peak currents and half-height widths vary as n^2 and $1/n$, respectively).[8] Intermolecular interactions (between active sites in adjacent adsorbed molecules) which are important for small molecules,[8] are expected to be negligible. On addition of substrate, these signals are replaced by catalytic waves—the current amplification depending on turnover rate. At sufficiently high coverage and at appropriately slow scan rates, diffusion of substrates to and from the adsorbed enzyme molecules will be linear; in this case, the use of a rotating disk electrode provides control of the flux of substrates (and products), and linear-sweep voltammetry yields steady-state currents with characteristic sigmoidallike waves. At very low coverages, i.e., below the level at which nonturnover signals can be detected, microelectrode array behavior is predicted that will also produce steady-state voltammetry even at a stationary electrode.[9,10] The shape, height, steepness, and potentials of representative features (e.g., half-wave potentials) are expected to be convoluted functions of substrate mass transport (concentration, diffusion, electrode rotation rate), kinetic characteristics (both electron transfer and associated chemical events), and thermodynamic properties (e.g., reduction potentials and substrate binding) of the enzyme at the interface.

Case A: The Basic Two-Electron Model

Our basic model is that of an enzyme having a two-electron active site but no internal "relay stations". This might be a simple flavoenzyme or a peroxidase [in which the oxidized state consists of Fe(IV)═O coupled to a cation radical]. The physiological electron donor/acceptor would be an outer-sphere agent such as an electron-carrier protein, but in our system it is a rotating disk electrode. To incorporate control over substrate mass transport by electrode rotation, we assume that the enzyme is adsorbed to a level of electroactive coverage (visible from nonturnover voltammetry) that yields linear diffusion characteristics. In this paper, we consider catalytic electron transfer occurring in the direction of substrate reduction: obviously an analogous theory will apply to oxidation.

The reactions occurring during turnover are shown in Scheme 1. Reversibility and cooperativity of the active-site reduction are included in the model by the equilibrium potentials E_1 and E_2 for the first and second reduction steps, respectively, and the interfacial electron-transfer rate constants k^{F}_{E1}, k^{B}_{E1}, k^{F}_{E2}, and k^{B}_{E1}, where superscripts F and B denote forward (reduction) and backward (oxidation) directions. The potential dependence of these rate constants is described by well-established electron-transfer models (see Appendix A) and the difference between E_1 and E_2 defines the stability of the one-electron reduced state. A single two-electron reduction of the active site occurs when $E_1 \ll E_2$,[3,8,11,12] but this cooperativity, observed under equilibrium conditions, does not exclude participation of the unstable one-electron reduced state during turnover (when $k^{\mathrm{F}}_{E2} \leq k^{\mathrm{F}}_{E1}$). Note that for simplicity the model is both sequential (substrate binds exclusively to the reduced state) and unidirectional (conversion of substrate to product is irreversible).

SCHEME 1 : Model Describing the Two-Electron Reduction of Substrate by an Enzyme Adsorbed at a Rotating Disk Electrode[a]

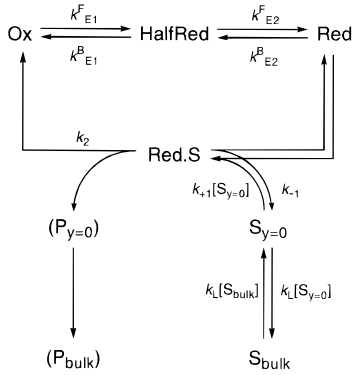

[a] The enzyme is reduced in two one-electron steps by the electrode. S is the substrate, P is the product, Ox is the fully oxidized enzyme, HalfRed is the one-electron reduced enzyme, Red is the fully reduced enzyme, and Red.S is the fully reduced enzyme with bound substrate.

Exchange of substrate between the bulk and the surface ($y = 0$) is defined by an apparent mass-transport rate constant, k_L. According to the Levich equation,[13] the steady-state, mass-transport limited current for reduction of S at a rotating disk electrode is

$$i = -0.620nFAD^{2/3}\omega^{1/2}\nu^{-1/6}([\mathrm{S_{bulk}}] - [\mathrm{S}_{y=0}]) \qquad (1)$$

where A is the electrode area (square centimeters), D is the diffusion coefficient (square centimeters per second), ω is the rotation rate (radians per second), ν is the kinematic viscosity (0.01 $\mathrm{cm^2\ s^{-1}}$ at 25 °C in water), and $[\mathrm{S_{bulk}}]$ and $[\mathrm{S}_{y=0}]$ are the substrate concentrations (moles per cubic centimeter) in bulk solution and near the electrode surface, respectively. Given that the net rate of transport of substrate to the surface, $k_{\mathrm{L}}([\mathrm{S_{bulk}}] - [\mathrm{S}_{y=0}])$, is equal to the turnover number (reciprocal seconds) at steady state, and with

$$i_{\mathrm{cat}}(E) = -nFA\Gamma_{\mathrm{total}} \times \text{turnover number} \qquad (2)$$

it follows that

$$k_{\mathrm{L}} = 0.620\frac{D^{2/3}\omega^{1/2}\nu^{-1/6}}{\Gamma_{\mathrm{total}}}\ \mathrm{mol^{-1}\ cm^3\ s^{-1}} \qquad (3)$$

where Γ_{total} is the surface coverage of active enzyme (moles per square centimeter). As derived in Appendix B, the steady-state turnover number is given by a modified form of the Michaelis−Menten equation:

$$\text{turnover number} = k_2/\left(1 + \frac{K^{\infty}_{\mathrm{M}}/H}{Q[\mathrm{S_{bulk}}]} + G\right) \qquad (4a)$$

where

$$K_M^{\infty} = (k_{-1} + k_2)/k_{+1} \quad (4b)$$

K_M^{∞} is equal to the Michaelis−Menten definition of K_M when electron transfer is not rate-limiting (and thus $k_2 = k_{cat}$). The terms H, G, and Q are defined as follows.

The term H describes the thermodynamic potential dependence of active-site oxidation states:

$$H = 1/(1 + \epsilon_2 + \epsilon_1\epsilon_2) \quad (5a)$$

where

$$\epsilon_i = \frac{k_{Ei}^B}{k_{Ei}^F} = \exp\left(\frac{F}{RT}(E - E_i)\right) \quad (5b)$$

At any applied potential E, H gives the maximum fraction of active sites that are in the reduced state ($\Gamma_{Red}/(\Gamma_{Ox} + \Gamma_{HR} + \Gamma_{Red})$) and thus able to bind substrate, and this results in a sigmoidal increase of the turnover number as the applied potential becomes more negative.

The term G is concerned with the kinetics of interfacial electron transfer:

$$G = k_2\frac{k_{E1}^F + k_{E2}^F + k_{E1}^B}{k_{E1}^F k_{E2}^F} = k_2\left(\frac{1}{k_{E1}^F} + \frac{1 + \epsilon_1}{k_{E2}^F}\right) \quad (6)$$

It becomes vanishingly small when the rate constants k_{E1}^F and k_{E2}^F are high. Obviously this condition is more readily fulfilled if there is strong electronic coupling (the redox center lies close to the electrode surface) but, more importantly, the potential dependence of the electron-transfer rate constants means that as a more negative potential is applied (higher overpotential), the rate constants for reduction (k_{E1}^F and k_{E2}^F) increase while those for oxidation (k_{E1}^B and k_{E2}^B) decrease. As a result, G decreases as the applied potential is made more negative.

The term Q describes depletion of the substrate at the electrode surface and reflects the net effectiveness of mass transport in replenishing the substrate that is converted:

$$Q = \frac{[S_{y=0}]}{[S_{bulk}]} = \frac{1}{2}\left(P + \sqrt{P^2 + \frac{K_M^{\infty}}{[S_{bulk}](1 + G)}}\right) \quad (7a)$$

where

$$P = 1 - \frac{K_M^{\infty}}{[S_{bulk}]}\frac{(1/H + 1/L)}{(1 + G)} \quad (7b)$$

and

$$L = k_L K_M^{\infty}/k_2 \quad (7c)$$

The normalized mass-transport parameter L is the ratio of the equivalent mass-transport rate constant, k_L, to the second-order rate constant for substrate conversion, k_2/K_M^{∞}. Q tends toward a maximum value of 1 at high mass-transport rates (high rotation rates), relative to the rate of depletion at the surface, or at high substrate concentrations.

Assuming that electron transfer is not limiting at high overpotential, the Koutecky−Levich approximation of the limiting current is given by

$$1/i_{lim} = 1/i_{cat} + 1/i_{Lev} \quad (8a)$$

with

$$i_{cat} = -nFA\Gamma_{total}k_2/(1 + K_M^{\infty}/[S_{bulk}]) \quad (8b)$$

and

$$i_{Lev} = -0.620nFAD^{2/3}\omega^{1/2}\nu^{-1/6}[S_{bulk}] \quad (8c)$$

This yields a current equivalent to eqs 2 and 4a (with $G = 0$ and $H = 1$ at $E \rightarrow -\infty$) but with a factor Q that is independent of substrate concentration:

$$Q(E \rightarrow -\infty) = 1/(1 + 1/L) \quad (9)$$

The limiting currents predicted by our model are higher than those predicted by the Koutecky−Levich approximation, and plots of $1/i_{lim}$ versus $1/\omega^{1/2}$ are expected to deviate from linearity at high rotation rates.[14]

We now consider three control regimes, assuming that there is no time (scan rate) dependence or restriction on the validity of the Levich equation at low and high rotation rates. Initially we will discuss limiting cases to illustrate the underlying principles, and all rate constants and currents will be given relative to k_2. Thus, the plotted trends for an increasing dimensionless rate constant can be regarded as effects either of increasing the appropriate rate constant or of decreasing the activity of the enzyme by decreasing k_2.

Mass-Transport Control. Mass-transport control occurs when the rate of supply of substrate to the enzyme is much smaller than the rate at which the active site can convert substrate, i.e., when $L < K_M^{\infty}/[S]$, and when interfacial electron transfer is fast relative to k_2 (G is very small). Voltammograms under these conditions are truly sigmoidal, with limiting currents increasing with electrode-rotation rate (i.e., with $\omega^{1/2}$) as predicted by eq 1. Strictly speaking, such a situation is only achieved at the hypothetical limits of zero rotation rate or infinitely fast k_2, i.e., when L or $[S_{bulk}]$ tend toward zero. In this case, the apparent n-value (steepness) equals 2, reflecting the stoichiometry of the substrate reaction. It should be noted that due to practical limitations, variation of the rotation rate cannot effect more then a 10-fold change of L; the order of magnitude of the current is thus largely determined by the surface coverage and efficiency of the enzyme.

Figure 2 shows how wave shapes and positions vary with L for the two extreme cases $E_2 > E_1$ (cooperative two-electron reduction) and $E_1 > E_2$ (stable HalfRed state), at $[S_{bulk}] = K_M^{\infty}$. The applied potential is given relative to the two-electron enzyme potential E_m [$= (E_1 + E_2)/2$]. The changes are more easily distinguished in the derivative form; the maximum derivative has been scaled to reflect the apparent n-value of the catalytic wave (see Appendix C, eq C3). As L increases (i.e., mass-transport control is relaxed), $E_{1/2}$ becomes more negative, and the shape and position of the wave starts to depend on substrate concentration and the cooperativity of the electron transfer. This reflects the increasing influence of the enzyme on the observed wave, as will be discussed below. Note the current magnitudes: for $L < 10^{-2}$ the wave is barely discernible relative to $L \geq 10$, and so the situation becomes of academic interest only.

When $[S_{bulk}] < K_M^{\infty}/L$ (i.e., $k_L[S_{bulk}] < k_2$), the substrate concentration near the electrode is negligible; hence the half-wave potential becomes independent of $[S_{bulk}]$, while the magnitude of the wave is proportional to $[S_{bulk}]$, at a given L. This reflects the irreversibility imposed by the unidirectional

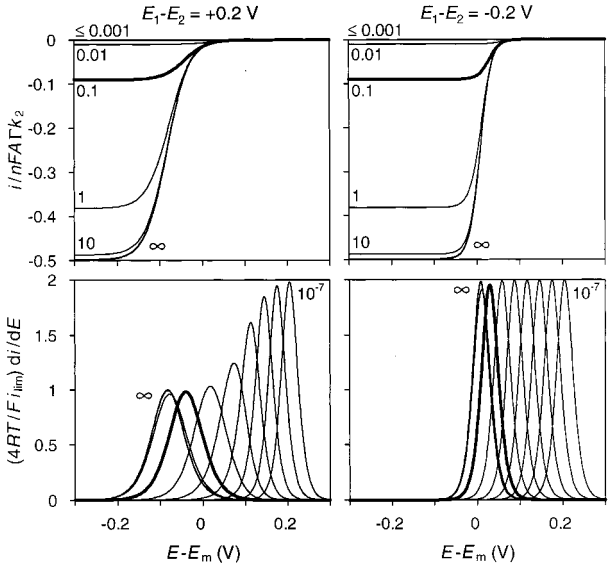

Figure 2. Effect of mass-transport control on the catalytic wave magnitude, shape, and position for the cases of a stable ($E_1 - E_2 = +0.2$ V) and an unstable ($E_1 - E_2 = -0.2$ V) half-reduced state of the active site. Shown are $L = 10^{-7}$, 10^{-6}, 10^{-5}, 10^{-4}, 10^{-3}, 0.01, 0.1, 1, 10, 100, and ∞ (i.e., $Q = 1$), for $[S_{bulk}] = K_M^{\infty}$; $T = 295$ K; $k_{E1}^F \gg k_2$ and $k_{E2}^F \gg k_2$ (i.e., $G \rightarrow 0$) for the plotted potential range. The normalized currents in the top panels show the magnitutes of the waves. Note that for $L < 0.01$ the currents are very small relative to $nFA\Gamma k_2$, and therefore not visible. The derivative voltammograms in the bottom panels are normalized to $4RT/Fi_{lim}$ (see eq C3) and show the shape and position of the waves. The bold traces ($L = 0.1$) show a typical example of a mass-transport controlled enzyme (100 rpm, $K_M = 0.1$ mM, $k_{cat} = 400$ s^{-1}, $\Gamma = 5$ pmol cm^{-2}, $D = 10^{-5}$ cm^2 s^{-1}, $\nu = 0.01$ cm^2 s^{-1}).

nature of k_2: our theoretical enzyme (Scheme 1) is infinitely biased to act in the reductive direction only. Under experimental conditions, the reverse reaction to k_2 is likely to occur at low rotation rates when product is accumulated at the electrode surface.

Enzyme Control. Without limitations due to mass transport ($L \rightarrow \infty$, $Q = 1$) or interfacial electron transfer (the limiting case of $G = 0$), the wave shapes, half-wave potentials, and low-potential limiting currents are determined only by the enzyme. In the simple case of our model we consider the parameters k_2 and K_M^{∞} according to the normal Michaelis−Menten equation, and the two one-electron reduction potentials E_1 and E_2.

Figure 3 shows how the shape and position of the limiting wave ($G = 0$, $L \rightarrow \infty$, $Q = 1$) vary with substrate concentration for the two extreme cases $E_1 > E_2$ and $E_2 > E_1$. At very low substrate concentrations ($\leq K_M^{\infty}/10$), the half-wave potential is determined by the potentials of the active site. For $E_2 > E_1$, the limiting wave is located at E_m and the shape is that of an $n = 2$ wave, whereas for $E_1 > E_2$ the limiting wave is found at E_2 and the shape is $n = 1$. The latter result appears at first to contradict expectations of a cooperative two-electron *substrate* reduction. However, this is a consequence of active-site thermodynamics (as reflected in term H). Turnover cannot occur before the potential is low enough for the active site to be fully reduced and able to bind a substrate molecule ($E < E_2$). The halfwave potential (at E_2) and the $n = 1$ shape of the wave merely reflect the Nernstian titration curve of the active site (since $\Gamma_{Red.S}$ is negligibly small when $[S_{bulk}] \ll K_M^{\infty}$).

Raising $[S_{bulk}]/K_M^{\infty}$ causes the waves to shift to higher potential. At limiting high substrate concentrations the n-value approaches 2 for all E_1 and E_2, and the half-wave potential is

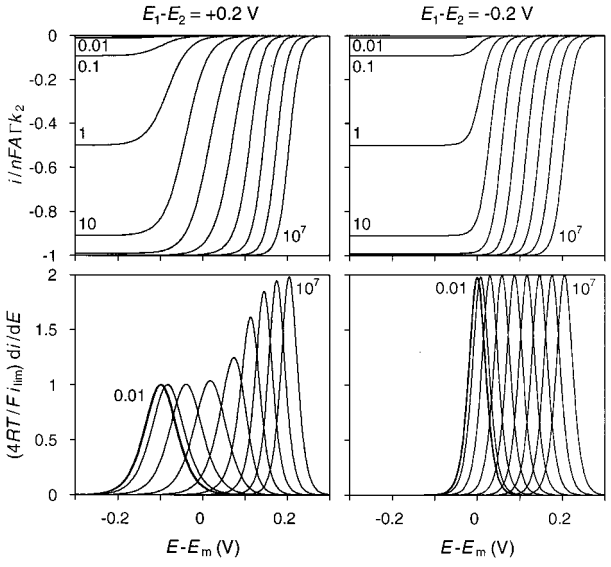

Figure 3. Effect of the substrate concentration on the catalytic wave magnitude, shape, and position for the cases of a stable ($E_1 - E_2 = +0.2$ V) and an unstable ($E_1 - E_2 = -0.2$ V) half-reduced state of the active site. Shown are $[S_{bulk}]/K_M^{\infty} = 10^7$, 10^6, 10^5, 10^4, 10^3, 100, 10, 1, 0.1, and 0.01 for $L \rightarrow \infty$ (i.e., $Q = 1$); $T = 295$ K; $k_{E1}^F \gg k_2$ and $k_{E2}^F \gg k_2$ (i.e., $G \rightarrow 0$) for the plotted potential range. Note that the normalized derivatives converge when $[S_{bulk}]/K_M^{\infty} \leq 0.1$.

given by

$$E_{1/2} = E_m + \frac{RT}{2F} \ln\left(1 + \frac{[S_{bulk}]}{K_M^{\infty}}\right) \qquad (10)$$

This reflects the binding of the substrate (which in our model binds exclusively to the fully reduced state). Because Γ_{Red} is negligibly small at high $[S_{bulk}]/K_M^{\infty}$, HalfRed is effectively directly reduced to Red.S, the thermodynamics of which we describe by an effective potential E_2*. With increasing substrate concentration E_2* shifts to more positive values, and once E_2* $> E_1$ a cooperative two-electron wave is observed. The wave remains close to E_m at experimentally reasonable values of $[S_{bulk}]/K_M^{\infty}$ (<10).

Figure 4 shows how the shape and position of the wave are influenced by the stability of the half-reduced state in the absence of limitations due to mass transport ($Q = 1$) or electron transfer (although this requires $G \rightarrow 0$ over the entire potential range and is thus hypothetical). The lower panel shows the Heyrovský-Ilkovic′ plots (see Appendix C), for which the limits at low and high potential are, respectively

$$\ln\left(\frac{i_{lim} - i}{i}\right) = \frac{F}{RT}(E - E_2) - \ln\left(1 + \frac{[S_{bulk}]}{K_M^{\infty}}\right) \qquad (11a)$$

for $E \ll E_1$ and

$$\ln\left(\frac{i_{lim} - i}{i}\right) = \frac{2F}{RT}(E - E_m) - \ln\left(1 + \frac{[S_{bulk}]}{K_M^{\infty}}\right) \qquad (11b)$$

for $E \gg E_1$. The apparent n-value, derived from the slope of the log plot, varies along the wave from $n = 2$ at high potential to $n = 1$ at low potential, and the measured value thus depends on where the wave is positioned relative to E_1 and E_2. The wave position, as we have seen, is influenced by substrate concentration, binding, and transport and will also be affected by interfacial electron transfer.

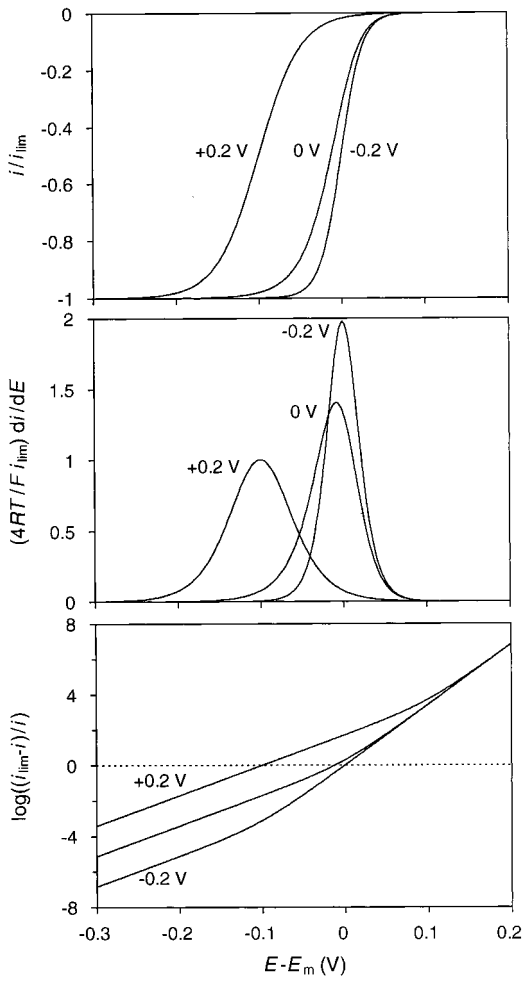

Figure 4. Effect of the thermodynamic stability of the half-reduced state on the shape and position of the catalytic wave. Shown are $E_1 - E_2 = 0.2$, 0, and -0.2 V, for $[S_{bulk}]/K_M^{\infty} = 0.01$, L $\rightarrow \infty$ ($Q = 1$); $T =$ 295 K; $k_{E1}^F \gg k_2$ and $k_{E2}^F \gg k_2$ (i.e., $G \rightarrow 0$) for the plotted potential range. The middle panel shows the normalized derivative voltammograms, and the bottom panel shows log $((i - i_{lim})/i)$.

Interfacial Electron-Transfer Control. As the interfacial electron-transfer rates decrease and start to influence the catalysis, the wave shifts to lower potentials and becomes distorted. Two different electron-transfer models, describing the potential dependence of the rate constants k_{E1}^F, k_{E1}^B, k_{E2}^F, and k_{E2}^B (see Appendix A) are considered: the (integrated) Marcus model and the symmetrical Butler−Volmer model (i.e., transfer coefficient $\alpha = 0.5$). The two models are compared for the case of high substrate concentration and rotation rate (i.e., in the absence of electron-transfer limitation, the waves are at high potential and have a pure $n = 2$ shape for all E_1 and E_2, as discussed previously and shown in Figure 3), and the electron-transfer rates at zero overpotential are equal for both one-electron steps (i.e., equal k_0 at $E = E_1$ and at $E = E_2$).

The Butler−Volmer Model. This describes exponentially increasing electron-transfer rates that eventually, at high overpotential, cease to limit catalytic turnover. The maximum (limiting) current is then determined by intrinsic properties of the enzyme (maximum turnover number at a given substrate concentration) or mass transport (for small values of L). Figure 5 shows that the wave gets less steep (the derivative decreases) and shifts to lower potential as the k_0 values decrease relative to k_2. The shift and broadening are analogous to that observed for polarographic waves when electron transfer is sluggish.[13] For $E_1 \gg E_2$, the derivative broadening and shift are monotonic,

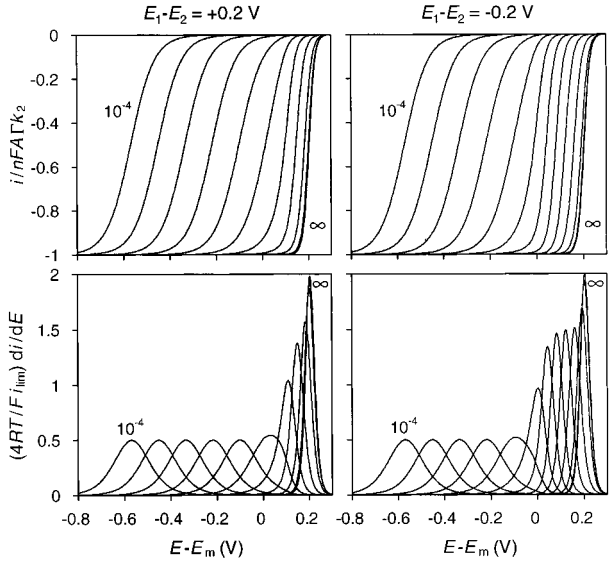

Figure 5. Effect of Butler−Volmer electron-transfer rates on the catalytic wave magnitude, shape, and position for the cases of a stable ($E_1 - E_2 = +0.2$ V) and an unstable ($E_1 - E_2 = -0.2$ V) half-reduced state of the active site. Shown are $k_{E1}^0/k_2 = k_{E2}^0/k_2 = k_0/k_2 = \infty$, 10^7, 10^6, 10^5, 10^4, 10^3, 100, 10, 1, 0.1, 0.01, 10^{-3}, and 10^{-4} for $\alpha_1 = \alpha_2 =$ 0.5, $[S_{bulk}]/K_M^{\infty} = 10^{+7}$, $L \rightarrow \infty$ (i.e., $Q = 1$), $T = 295$ K.

but for $E_1 \leq E_2$ an intermediate plateau is observed at $n = 1 + \alpha$ (i.e., 1.5 for $\alpha = 0.5$). An asymmetry is also apparent at intermediate k_0/k_2.

When $E_1 < E_2$ and the second electron transfer is fast, the HalfRed state is both thermodynamically and kinetically unstable. We might initially expect the model to predict behavior equivalent to that produced by a single two-electron reduction, and without electron-transfer limitations the models do indeed converge. However, when k_{E1}^F becomes rate-limiting, the predicted behavior is different: for a single two-electron transfer, the derivative peak is twice as sharp ($n = 1$ for $\alpha = 0.5$) in the limit of $k_0/k_2 < 0.1$, and the halfwave potential shifts half the extent of the two-step model. This is caused by the different potential dependence of the limiting electron-transfer rate: a true two-electron rate-limiting step [$n = 2$ in the Butler−Volmer equation (eq A7)] with zero overpotential at $E = E_m$ is obviously different from a one-electron rate-limiting step ($n = 1$ in eq A7) with zero overpotential at $E = E_1$. We have chosen to discuss primarily the $2\times$ $n = 1$ model because it includes noncooperative cases, and because in biological systems long-range interfacial electron-transfer most often occurs in one-electron steps, even when the active-site reduction is cooperative.

The plateau at intermediate k_0/k_2 is only observed for $E_1 \leq E_2$ when the second electron-transfer step is slow or rate-limiting and the resulting half-wave potential is between E_1 and E_2, i.e., when the electron-transfer rate influences the wave but the fraction of HalfRed is still small. We interpret this behavior in terms of a tradeoff between kinetic accumulation and thermodynamic instability of the HalfRed state, which results in $n_{app} = 1 + \alpha$ for electron-transfer rates where the fraction HalfRed is still small.

For very sluggish electron transfer ($k_0/k_2 < 0.1$), the derivative is symmetrical and broad ($n_{app} = 0.5$, reflecting $\alpha n = 0.5$ in eq A7). Decreasing k_0 causes no further change in shape, but the potential continues to shift. This is observed for all $E_1 - E_2$, and also when $k_{E1}^0 \rightarrow \infty$ or $k_{E2}^0 \rightarrow \infty$, because the potential dependence of the rate-limiting step(s) is similar (same α) and thus will have the same net result on the shape of the turnover

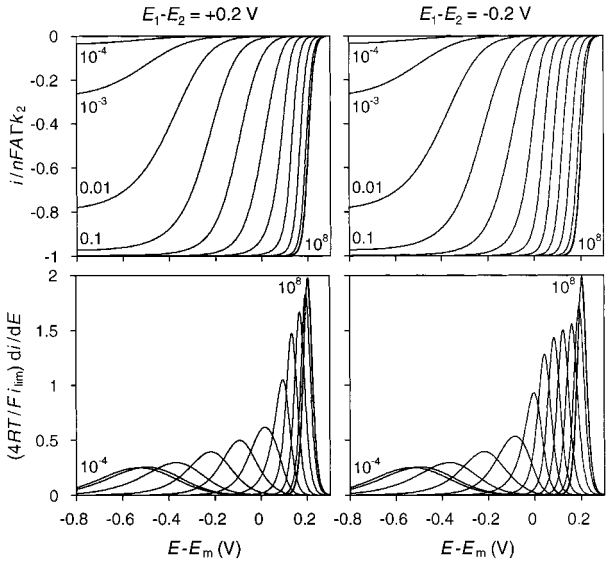

Figure 6. Effect of Marcus electron-transfer rates on the catalytic wave magnitude, shape, and position for the cases of a stable ($E_1 - E_2 = +0.2$ V) and an unstable ($E_1 - E_2 = -0.2$ V) half-reduced state of the active site. Shown are $k^0_{E1}/k_2 = k^0_{E2}/k_2 = k_0/k_2 = 10^8$, 10^7, 10^6, 10^5, 10^4, 10^3, 100, 10, 1, 0.1, 0.01, 10^{-3}, and 10^{-4} for $\lambda_1 = \lambda_2 = 0.5$ eV, $[S_{bulk}]/K^{\infty}_M = 10^{+7}$, $L \rightarrow \infty$ (i.e., $Q = 1$), $T = 295$ K.

versus potential curve. We note that when the k_0 values are equal, the electron transfer is most efficient for $E_1 = E_2$.

The Marcus Model. By contrast with the Butler−Volmer model, Marcus theory predicts a *sigmoidally* increasing electron-transfer rate, the important implication being that when $k_{max} \ll k_2$, the observed maximum (limiting) current may arise from slow interfacial electron-transfer rather than enzyme kinetics. The problem is how to distinguish between these two cases. Figure 6 shows that with decreasing k_0/k_2 (and proportionally decreasing k_{max}/k_2: at reorganization energy $\lambda = 0.5$ eV, $k_{max} = 758\ k_0$) the limiting current decreases, and the derivative broadens and shifts to lower potential. The latter effect is more pronounced for higher λ, and for $\lambda > 0.1$ eV the derivatives at low k_0/k_2 are broader than the Butler−Volmer model predicts. The Marcus model also predicts the intermediate plateau at $n = 1.5$ (when $E_1 \leq E_2$), the extent of which is increased at higher λ. At very high λ (>1 eV), a second plateau becomes visible at $n = 0.5$, the extent of which again increases with λ (for $\lambda \rightarrow \infty$, equivalent to Butler−Volmer, this results in an observed limiting value $n = 0.5$). The variation of the half-wave potentials with k_0/k_2 for different values of λ (including $\lambda \rightarrow \infty$, equivalent to Butler−Volmer) are shown in Figure 7. The half-wave potential reaches a lower limit close to $E = E_m - \lambda$ at low electron-transfer rates (hence the absence of such a limit with the Butler−Volmer model). This limiting half-wave potential and the low n-values observed as electron transfer becomes fully limiting each reflect the potential dependence of the interfacial electron-transfer rates: for Marcus theory the rate reaches 50% of its maximum value at $E = E^{\circ} - \lambda$, with the slope of the sigmoidal decreasing as λ increases.

Case B: Sequential Two-Electron Model Involving an Intramolecular Relay System

We now consider the situation that arises when the active site is dependent upon an *intramolecular* relay system consisting of two electron-transfer centers C1 and C2. For biological efficiency, such "relay stations" have probably been positioned within enzymes so as to optimize rates of electron transport

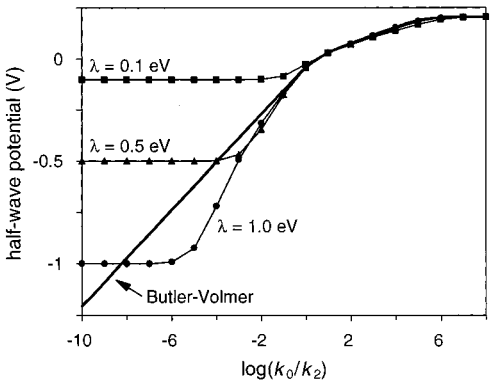

Figure 7. Half-wave potentials versus electron-transfer rate constants at different reorganization energies. Conditions: $\lambda_1 = \lambda_2$, $E_1 = E_2 = 0$ V, $k^0_{E1}/k_2 = k^0_{E2}/k_2 = k_0/k_2$, $[S_{bulk}]/K^{\infty}_M = 10^{+7}$, $L \rightarrow \infty$ (i.e., $Q = 1$), $T = 295$ K.

SCHEME 2 : Extension of Scheme 1, Replacing Direct Electron Transfer from the Electrode to the Active Site by Relay of Electrons via Either of Two One-Electron Centers (C1 and C2)

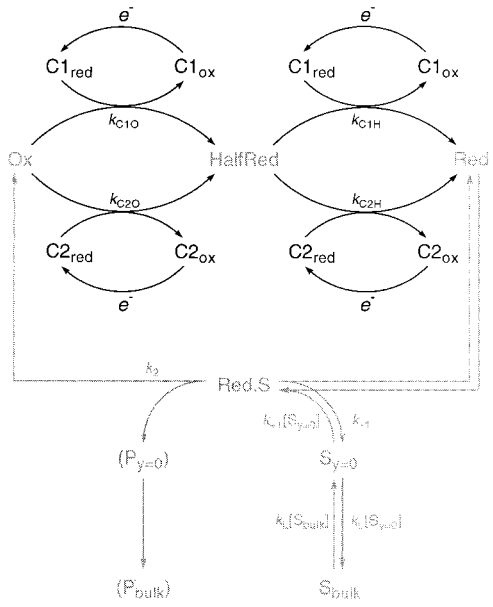

between the active site and external redox partners.[2] In our model, these centers mediate one-electron reactions (to and from the electrode) that transform the active site between Ox, HalfRed, and Red states and may be rate-determining. The reactions occurring during turnover are shown in Scheme 2. For simplicity, we assume that electron transfer between the electrode and C1 or C2 is reversible in the electrochemical sense, i.e., $k_0 \gg k_2$, and the populations of these centers obey the Nernst equation at all times. The active-site reduction rate constants can therefore be calculated by multiplying the rates of electron transfer from fully reduced center C1 or C2 to Ox or HalfRed by the fraction of reduced C1 or C2. The resulting rate constants for reduction of the active site are thus given by

$$k^{F}_{E1} = \frac{k_{C1O}}{1 + \epsilon_{C1}} + \frac{k_{C2O}}{1 + \epsilon_{C2}} \tag{12a}$$

and

$$k^{F}_{E2} = \frac{k_{C1H}}{1 + \epsilon_{C1}} + \frac{k_{C2H}}{1 + \epsilon_{C2}} \tag{12b}$$

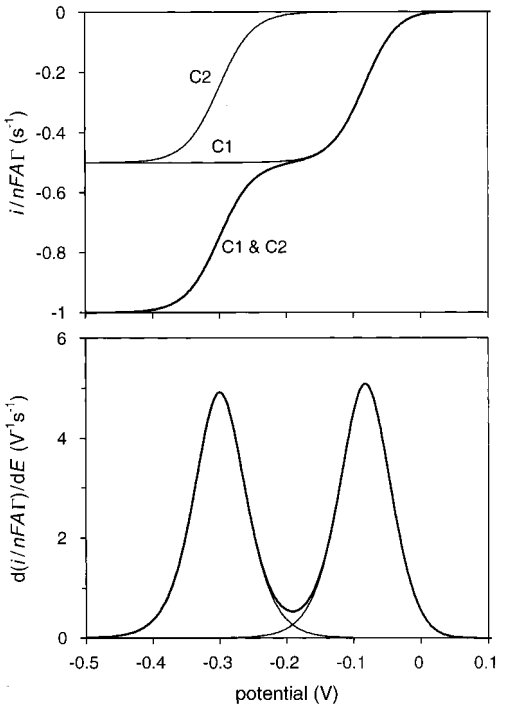

Figure 8. Turnover number as a function of potential for three cases of fully rate-limiting electron relay. Conditions: $L \rightarrow \infty$, $[S] = K_M^{\infty}$, $k_2 = 10^6$ s^{-1}, $E_1 = -0.1$ V, $E_2 = +0.1$ V, $E_{C1} = 0$ V, $E_{C2} = -0.3$ V, $T = 295$ K. C1: $k_{C1O} = k_{C1H} = 1$ s^{-1} and $k_{C2O} = k_{C2H} = 0$ (i.e., a single high-potential relay); C2: $k_{C1O} = k_{C1H} = 0$ and $k_{C2O} = k_{C2H} = 1$ s^{-1} (i.e., a single low-potential relay); C1 and C2: $k_{C1O} = k_{C1H} = k_{C2O} = k_{C2H} = 1$ s^{-1} (i.e., two relay sites).

with

$$\epsilon_{Ci} = \exp\left(\frac{F}{RT}(E - E_{Ci})\right) \tag{13}$$

where E_{Ci} is the equilibrium reduction potential of center C1 ($i = 1$) or C2 ($i = 2$). When eqs 12 and 13 are used to describe the relations between the applied potential and the active-site reduction rates, the turnover number is again described by eq 4.

Figure 8 displays three examples of cases where electron relay is very slow compared to the maximum turnover number of the active site. The relay model predicts two catalytic waves when electron relay is rate-limiting, and a second center with a lower reduction potential increases the total electron relay rate. In Table 1, the main features of the catalytic waves (shapes, positions) for these and other extreme cases of fully rate-limiting electron relay (i.e., for an extremely active catalytic site and high electrode rotation rate) and $E_1 < E_2$ (cooperative active-site potentials) are presented as example quantities. The first nine rows refer to cases in which some of the relay rates are absent (zero rates) while the other steps are slow. These cases show that two waves are predicted only when C1 mediates both reduction steps but C2 is able to mediate at least one, thus boosting the overall reduction rate. The next 12 rows show that when one of the reduction steps is fast, two waves are predicted when the rate-limiting step is mediated by both centers.

In all cases for which a low-potential second wave is observed, its half-wave potential is close to the reduction potential of C2. The position of the high-potential wave (the derivative peak potential E_{p1}) is influenced by the reduction potentials both of the active site and of C1 and falls into three

TABLE 1: Example Quantities of Catalytic Waves Resulting from Rate-Limiting Electron Relay[a]

Ox → HalfRed		HalfRed → Red							
k_{C1O} (s^{-1})	k_{C2O} (s^{-1})	k_{C1H} (s^{-1})	k_{C2H} (s^{-1})	TO_{lim} (s^{-1})	E_{p1} (mV)	n_1	E_{p2} (mV)	n_2	i_2/i_{lim}
1	0	1	0[b]	0.50	−82	1.0			0
0	1	0	1[b]	0.50			−300	1.0	1
1	0	0	1	0.50			−282	1.0	1
0	1	1	0	0.50			−282	1.0	1
1	1	0	1	0.67			−294	1.0	1
0	1	1	1	0.67			−294	1.0	1
1	1	1	0	0.67	−82	1.0	−290	1.0	0.25
1	0	1	1	0.67	−82	1.0	−290	1.0	0.25
1	1	1	1[b]	1.00	−82	1.0	−300	1.0	0.50
∞	*x*	1	0	1.00	−100	1.0			0
x	∞	1	0	1.00	−100	1.0			0
x	∞	1	1	2.00	−100	1.0	−300	1.0	0.50
∞	*x*	1	1	2.00	−100	1.0	−300	1.0	0.50
∞	*x*	0	1	1.00			−300	1.0	1
x	∞	0	1	1.00			−300	1.0	1
1	0	∞	*x*	1.00	0	1.0			0
1	0	*x*	∞	1.00	0	1.0			0
1	1	∞	*x*	2.00	0	1.0	−300	1.0	0.50
1	1	*x*	∞	2.00	0	1.0	−300	1.0	0.50
0	1	∞	*x*	1.00			−300	1.0	1
0	1	*x*	∞	1.00			−300	1.0	1

[a] Conditions: No mass transport limitations ($L \rightarrow \infty$, $Q = 1$), $[S_{bulk}] = K_M^{\infty}$, $k_2 = 10^6$ s^{-1}, $E_1 = -0.1$ V, $E_2 = +0.1$ V, $E_{C1} = 0$ V, $E_{C2} = -0.3$ V, and $T = 295$ K. *x* stands for any value (from 0 to ∞); TO_{lim} is the turnover number at low potential; E_{p1} and E_{p2} are the derivative peak potentials (potential where the slope of the wave is maximum); i_2/i_{lim} is the relative contribution of the second wave to the limiting current. [b] These cases are plotted in Figure 8.

categories: $E_{p1} = E_1$ when the second reduction step is rate-limiting due to slow electron relay; E_{p1} is approximately equal to E_1 when both reduction steps are rate-limiting; and $E_{p1} = E_{C1}$ when the first reduction step is rate-limiting. Figure 9 shows how the wave shapes (*n*-values) and positions (derivative peak potentials), derived from simulations with only a single relay center (i.e., $k_{C2O} = k_{C2H} = 0$), depend on the reduction potential of the relay center. When the first reduction step is rate-limiting (top panel) and E_{C1} is low, the half-wave potential is equal to E_{C1} and the wave has an $n = 1$ shape. However, as E_{C1} increases to values more positive than the greater of E_1 and E_2, the *n*-value increases and the half-wave potential becomes constant (maximum values depend on the relay rate, active-site potentials, and enzymatic parameters). When the second reduction step is rate-limiting (bottom panel), the half-wave potential is equal to either E_{C1} or E_1, whichever is lowest, and the *n*-values always remain close to 1.

Observation of $n = 1$ wave shapes, even when the first electron relay is rate-limiting, may appear counterintuitive for a cooperative two-electron reduction. In our model, however, the relay rates are proportional to the Nernstian fraction of reduced relay site. This implies that when the reduction potential of the one-electron relay site is lower than that of the one-electron couples of the active site (Ox to HalfRed, HalfRed to Red), the rate as a function of potential shows the $n = 1$ characteristics and potential dependence of the mediator. The characteristics of the active site are thus obscured. Only when the mediator reduction potential is higher than that of the acceptor (Figure 9), or when the rate of electron relay is very fast (shown in Figure 10) do these characteristics become apparent. In the latter case, the relay model converges to the direct electron-transfer model of Scheme 1. For the limiting examples given in Figure 8 and in Table 1, neither of these two conditions is met, and all *n*-values are close to 1.

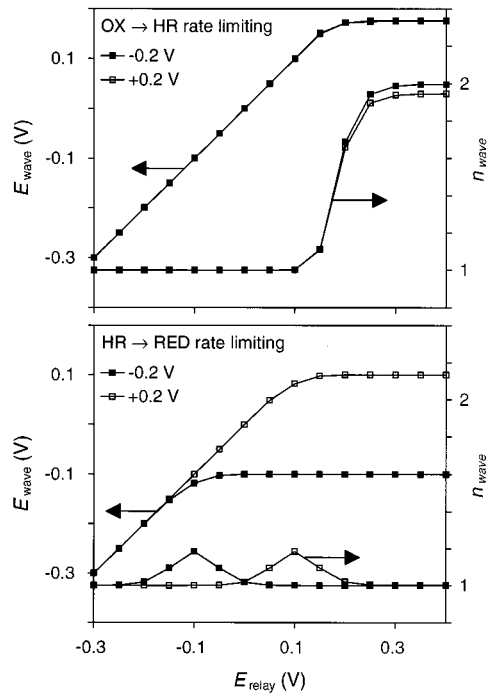

Figure 9. Effect of the reduction potential of a single relay center on wave positions (peak potentials of the derivative voltammograms) and shapes (*n*-values). Top panel, $k_{C1O} = 1\ s^{-1}$ and $k_{C1H} = \infty$; bottom panel, $k_{C1O} = \infty$ and $k_{C1H} = 1\ s^{-1}$. (□) $E_1 - E_2 = +0.2$ V; (■) $E_1 - E_2 = -0.2$ V. Other conditions: $L \rightarrow \infty$, $[S] = K_M^{\infty}$, $k_2 = 10^6\ s^{-1}$, $E_m = 0$ V, $T = 295$ K. The arrows indicate the vertical axis to which the traces are plotted.

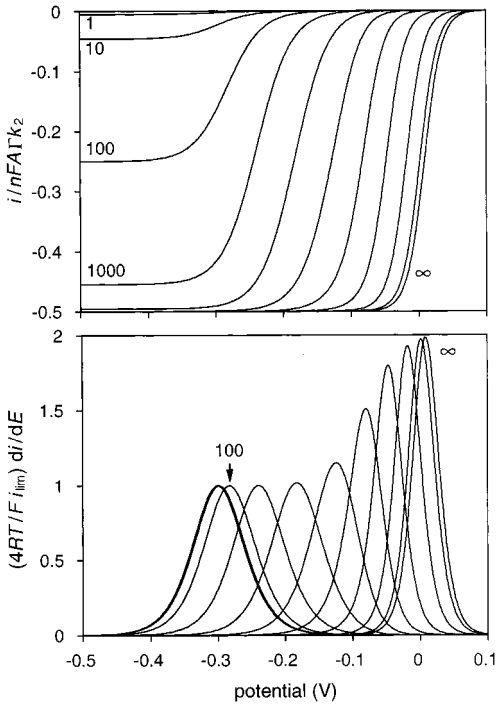

Figure 10. Effect of the relay rates on the magnitude, shape, and position of the catalytic waves. Shown are $k_{C1O} = k_{C1H} = 1$, 10, 100, 10^3, 10^4, 10^5, 10^6, 10^7, 10^8, 10^9, and $\infty\ s^{-1}$. Conditions: $k_{C2O} = k_{C2H} = 0$ (i.e., one relay only), $L \rightarrow \infty$, $[S] = K_M^{\infty}$, $k_2 = 100\ s^{-1}$, $E_1 = -0.1$ V, $E_2 = +0.1$ V, $E_{C1} = -0.3$ V, $T = 295$ K.

Mixed Mass-Transport and Electron-Transfer Control. The two models described as cases A and B predict a region where both mass transport and electron transfer from the electrode to the active site, either direct (Scheme 1) or relayed (Scheme 2), are slow compared to the activity of the enzyme. This situation has little utility for determining enzyme properties, but nonetheless it is necessary to recognize the problems that may arise. At given electron-transfer or relay rate constants, the height, shape, and position of the wave changes with rotation rate. When L is high, pure electron-transfer limited waves are observed, with $n \leq 2$ as discussed above. However, at intermediate L, mass-transport and electron-transfer rates will become comparable, and one will take over from the other as limiting factor as the potential becomes lower. Apparent *n*-values >2 are predicted because, within the wave, an abrupt transition takes place from electron-transfer rate limitation at high potential to mass-transport rate limitation at low potential. This gives the derivative peaks the appearance of being sharply "cut off", dropping back to zero almost vertically at a potential that increases with decreasing L. The maximum *n*-value is predicted to be higher with slower electron transfer. At extremely low L (which, obviously, is difficult to achieve experimentally without breakdown of the steady-state Levich concentration profile) the wave is limited purely by mass transport, and thus $n = 2$ is predicted. ($n > 2$ is not predicted for mixed mass-transport and *enzyme* control because the turnover is modulated by binding, i.e., availability of substrate.)

Discussion

In light of the predictions made, we now discuss some experimental results obtained for enzymes corresponding to each of the two cases described above; i.e., cytochrome *c* peroxidase, an example of case A, and fumarate reductase, an example of case B.

Cytochrome *c* Peroxidase. Cytochome *c* peroxidase (C*c*P) from bakers' yeast catalyzes the reduction of hydrogen peroxide to water by cytochrome *c*:

$$H_2O_2 + 2\ \text{cytochrome } c(Fe^{2+}) + 2\ H^+ \rightarrow 2\ H_2O + 2\ \text{cytochrome } c(Fe^{3+}) \quad (14)$$

The enzyme contains a single heme group. In the catalytic cycle, the Fe(III) or "resting" form binds hydrogen peroxide and is converted to the fully oxidized form, known as compound I, which features a ferryl heme Fe(IV)═O coupled to a cation radical formed on a proximal residue, tryptophan (Trp191). The resting form is regenerated by two sequential one-electron reactions, via an intermediate known as compound II, which can exist in two forms: [Fe(IV):Trp^0] and [Fe(III):$Trp^{\bullet +}$].[15,16] When C*c*P is adsorbed from cold, dilute (<1 μM) solutions at a pyrolytic graphite edge (PGE) rotating disk electrode, it can be reversibly oxidized by two electrons and is active in hydrogen peroxide turnover.[17] In the absence of hydrogen peroxide in the solution, a nonturnover signal consisting of a pair of oxidation and reduction peaks is observed, with a reduction potential $E_m = +736$ mV at pH 5.8. From the peak widths at half-height of 61 ± 5 mV it follows that $E_1 \approx E_2$ (assuming no dispersion).[3,8,11] The coverage of C*c*P approaches that expected for a monolayer, and in accordance with the predictions for linear diffusion, a sharp peaklike catalytic current is observed upon addition of low levels of H_2O_2 to the cell, with the electrode stationary.[18] However, when the electrode is rotated, the peaks transform into a sigmoidal catalytic reduction wave with a half-wave potential very close to E_m.[17] The shape and magnitude of this response is very sensitive to rotation rate, thereby showing that catalysis is largely mass-transport

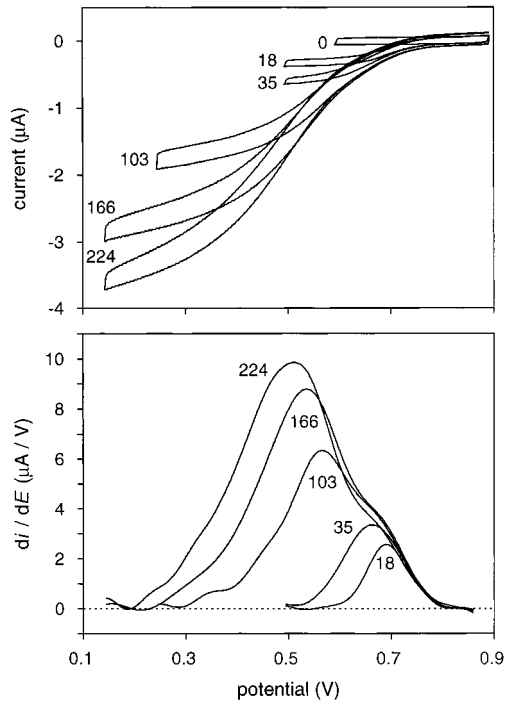

Figure 11. Catalytic voltammograms of adsorbed yeast C*c*P in the presence of 0, 18, 35, 103, 166, and 224 μM H_2O_2. Conditions: T = 4 °C, pH 5.8, rotation rate 450 rpm, electrode area 0.03 cm^2, scan rate 20 mV/s. The bottom graph shows the derivatives d*i*/d*E* of the scans in reductive direction after subtraction of noncatalytic background current (approximated by a second-order polynomial to correct for the slopes in the zero and limiting current regions).

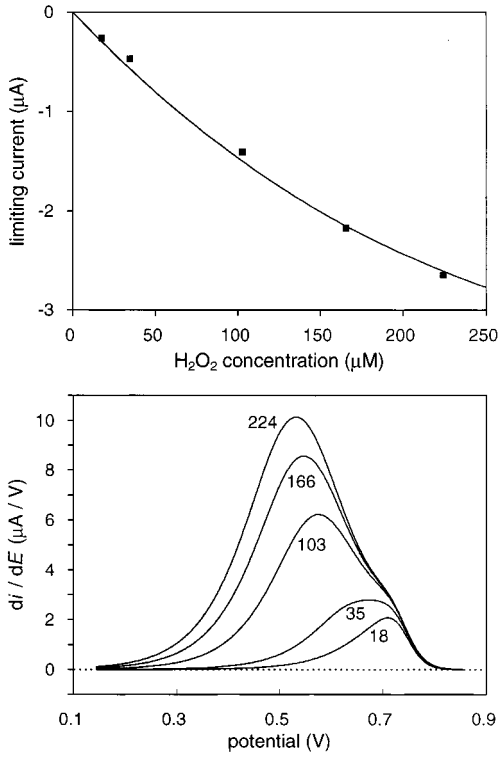

Figure 12. Modeling of yeast C*c*P catalytic voltammetry by Scheme 1, using the conditions given in Figure 11, K_M^{app} = 123 μM, k_{cat} = 311 s^{-1}, $E_1 = E_2$ = +736 mV, D = 1.4 10^{-5} cm^2 s^{-1}, and ν = 0.01 cm^2 s^{-1}. The top graph shows the measured limiting catalytic currents corrected for background (symbols), and the predicted currents (line) when Γ = 2.72 pmol cm^{-2}. The bottom graph shows the derivatives d*i*/d*E* of the predicted waves for $k_2 = 10^{10}$ s^{-1}. The first reduction step is very fast ($k_0 = 10^{20}$ s^{-1}, α = 0.5), and the second reduction step is modeled using eq 19 with k_0 = 7.69 s^{-1}, α = 0.348, and k_{chem} = 311.0 s^{-1} ($\approx k_{cat}$).

controlled (see Figure 2). In the example shown in Figure 11, the waves broaden significantly and shift to lower potentials when more peroxide is added (at constant rotation rate) and two components become distinguishable in the wave, as noted by a shoulder on the high-potential side of the derivative peaks. The model described in case A predicts these observations when electrochemical reduction of compound I back to the resting form is limited by a chemical step.

With tryptophan-191 treated as an integral part of the active site, the electrocatalytic peroxide reduction essentially follows Scheme 1 when Ox is compound I, HalfRed is compound II, Red is the resting Fe(III) form of C*c*P, and Red.S is the Michaelis complex, i.e., Fe(III) with bound H_2O_2. When electron transfer at low potential is not rate-limiting, $k_2 = k_{cat}$ and $K_M^{\infty} = K_M^{app}$. In general, however, k_2 might not be the (only) rate-limiting step as $E \rightarrow -\infty$ (e.g., in the case of Marcus-type electron transfer with low maximum rate constants, or gated electron transfer), and thus

$$1/k_{cat} = 1/k_2 + 1/k_{E1}^{max} + 1/k_{E2}^{max} \quad (15)$$

With factor G at infinite overpotential

$$G_{lim} = k_2(1/k_{E1}^{max} + 1/k_{E2}^{max}) \quad (16)$$

it follows that

$$k_2 = k_{cat}(1 + G_{lim}) \quad (17)$$

and when $k_2 \gg k_{-1}$

$$K_M^{\infty} \approx K_M^{app}(1 + G_{lim}) \quad (18)$$

Substitution of eqs 17 and 18 in eqs 4−7 shows that $k_2 = k_{cat}$, $K_M^{\infty} = K_M^{app}$, and $G_{lim} = 0$ can be used to calculate the current at $E \rightarrow -\infty$, independent of the real rate-determining step. The top panel of Figure 12 shows that the limiting currents are in agreement when Γ = 2.7 pmol cm^{-2}, using k_{cat} = 311 s^{-1} and K_M^{app} = 123 μM as determined separately at pH 5.8 by analyzing the limiting currents at various rotation rates and H_2O_2 concentrations.[19]

With Butler−Volmer electron-transfer rates (i.e., not limiting at low potential, and thus $k_2 = k_{cat}$ as observed for the adsorbed enzyme), the Scheme 1 model accounts for the shape and position of the measured waves when the second electron-transfer step is slow ($k_0 \sim 10$ s^{-1}). The shoulder is more pronounced at lower α and is almost absent when α = 0.5. However, the fact that the electrochemical k_{cat} is much lower than observed rates of compound I formation by H_2O_2[20] implies that regeneration of the resting state is rate-determining. Marcus theory also predicts a limiting electron-transfer rate, but λ must be very low (<0.2 eV) for either the first or the second step to approximate the observed peak widths and positions. This is more likely to reflect limitation by a coupled reaction rather than k_{max}. Moreover, the electron-transfer rates are symmetrical, i.e., equivalent to α = 0.5, at low overpotential where the rates are exponential in form, and so the experimentally observed shoulder is not predicted.

The potential dependence of the rate of peroxide reduction can be accounted for within the context of Scheme 1, employing the Butler−Volmer formulism to describe the interfacial electron transfer and including a limiting chemical event with first-order

rate constant k_{chem}:

$$k_{ET}^{app} = \left(\frac{1}{k_0 \exp(-\alpha F(E - E^0)/RT)} + \frac{1}{k_{chem}}\right)^{-1} \quad (19)$$

Good fits to the data, and particularly to the shape, height, and potential of the shoulder, can only be obtained when the first reduction step is fast, and either the first or the second reduction step is limited by $k_{chem} \approx k_{cat}$. The following two solutions are found: (i) between 0.1 and 0.9 V the first reduction rate constant is limited by k_{chem} ($k_0 \gg k_{chem}$), while the second step follows the Butler−Volmer model with $k_0 = 7.6\ s^{-1}$ and $\alpha = 0.35$ (not limited by a chemical step, i.e., k_{cat} is limited by $k_{E1}^F = k_{chem}$); and (ii) the first step is fast ($k_0 \gg k_{cat}$, no limiting chemical step), and the second step is modeled by using eq 19, with $k_{chem} \approx k_{cat}$, $k_0 = 7.7\ s^{-1}$, and $\alpha = 0.35$. The bottom panel of Figure 12 shows the resulting derivatives obtained for solution ii. The equivalence of the two solutions suggests that the rate-limiting chemical step is located between the reduction steps: compound I is quickly reduced by one electron, and compound II undergoes a rate-determining chemical transformation before further reduction to the resting state.[21]

The optimum apparent rate constant k_0 for the overall two-electron reduction is around $7\ s^{-1}$ for all the tested electron-transfer models. This is close to values measured in the absence of H_2O_2 by cyclic voltammetry in which the nonturnover signals are studied.[19] The rapid first reduction step predicted by the model can probably be assigned to the reduction of $Trp^{\bullet +}$, which has been reported to be very fast.[16,22] In reality, the asymmetric $\alpha = 0.35$ for the second reduction step probably reflects a second gating reaction, and the less optimal fit at the lowest substrate concentrations suggest that this gating is relaxed (i.e., α increases to 0.5) at low turnover numbers.

Fumarate Reductase. We have studied the voltammetry of the soluble catalytic subcomplex (FrdAB) of fumarate reductase from *Escherichia coli*.[3,5] This enzyme contains a stable, covalently bound flavin (FAD) at the active site, and catalyses the reduction of fumarate:

$$\text{fumarate} + 2\,e^- + 2\,H^+ \rightleftarrows \text{succinate} \quad (20)$$

In addition, three electron relay centers are present: a [2Fe-2S] cluster (center 1), a [4Fe-4S] cluster (center 2), and a [3Fe-4S] cluster (center 3). The enzyme adsorbs to approximately monolayer coverage on a PGE rotating disk electrode, and signals are observed that can be assigned to all four redox-active centers. The reduction potentials of centers 1 and 3 are close to that of the sharp two-electron FAD signal at pH 7 (−50 mV), while center 2 has a potential of −320 mV. Low concentrations of fumarate produce a single two-electron catalytic wave, close to the FAD potential and sensitive to rotation rate, again as expected for system dominated by mass-transport control (Figure 2). As with C*c*P (see above), if the electrode is not rotated, introduction of fumarate produces an intense catalytic peak, showing (as expected) that linear diffusion conditions apply for fumarate mass transport.[5] As conditions are altered to decrease the limitations of mass transport (increasing the fumarate concentration and rotation rate or using a higher pH, at which the enzyme is less active), a second catalytic wave appears, having a half-wave potential close to the potential of center 2. This wave contributes significantly to the total activity (24% at pH 9.5 with 0.8 mM fumarate). The steepness of the first wave decreases to $n < 1$ with increasing limiting current, while the second wave invariably has a one-electron shape. An example of the rotation rate dependence is shown in Figure 13. On the basis of the observed potentials, shapes (*n*-values), and the relative magnitudes of the waves at different conditions, we proposed that center 2 can provide an alternative relay operative at more negative potential.[3,5]

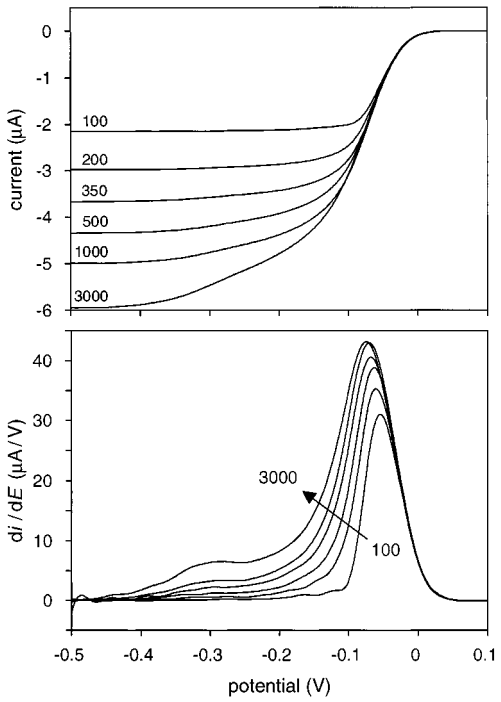

Figure 13. Catalytic voltammograms of *E. coli* FrdAB, adsorbed at a PGE, rotating at 100, 200, 350, 500, 1000, and 3000 rpm, in the presence of 0.2 mM fumarate (pH 7.0, 20 °C, electrode area 0.03 cm^2, scan rate 10 mV/s.). The traces shown are the first reductive scans on fresh films for each rotation rate, corrected for nonfaradaic backgrounds and adjusted to equal coverage using, as reference, a short excursion to 3000 rpm at low potential during the second scan. The bottom graph shows the derivatives d*i*/d*E*.

The aim of modeling the catalytic voltammetry of fumarate reductase is to ascertain the validity of the dual relay model. Scheme 2 is appropriate, once it is assumed that electron exchange between the electrode and the FeS clusters is facile, and the FAD does not interact directly with the electrode. Naturally, to use Scheme 2, we have also needed to assume that, in addition to center 2, only one of the high-potential clusters directly relays electrons to the flavin. Nominally, we have assumed that this is center 1 (noting that center 3 could provide a fast and thus nonlimiting relay between the electrode and center 1). Since fumarate reductase also has weak succinate dehydrogenase activity, Scheme 2 only applies when no succinate is present in bulk solution.

We now adjust the parameters of the model to reproduce limiting currents, contributions (relative and absolute) of the second wave, and derivative peak positions and widths, measured at pH 7 (with 0.2 mM fumarate at rotation rates of 100−3000 rpm and with 0.01−0.8 mM fumarate at 2000 rpm). Data analysis is described in Appendix C. For simplicity, equal relay rates for both electrons are assumed ($k_{C1O} = k_{C1H}$ and $k_{C2O} = k_{C2H}$). The following strategy is adopted to optimize parameters: First, D and Γ are optimized to obtain the correct limiting currents (with $K_M^{app} = 161\ \mu M$ and $k_{cat} = 840\ s^{-1}$ as reported for FrdAB)[5] by the method described above for C*c*P. Second, the relative amplitude of the second wave is optimized by adjusting the relay rate for center 2 relative to that for center 1 (i.e., k_{C2O}/k_{C1O}) for several given values of $G_{lim} = k_2/k_{relay}^{max}$,

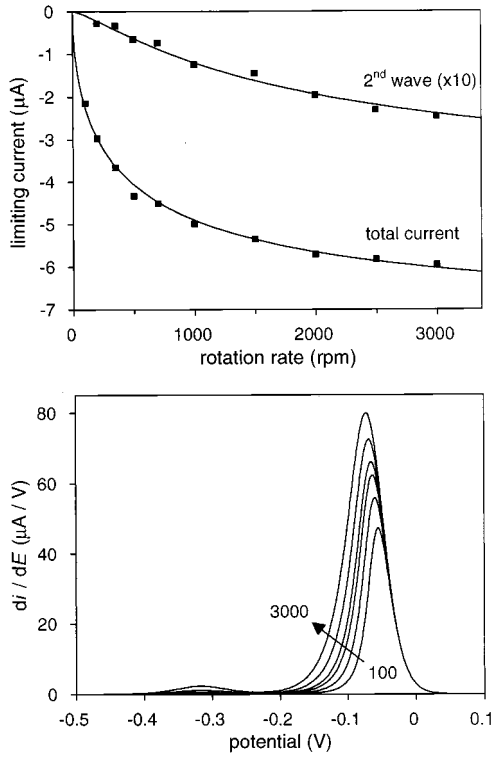

Figure 14. Modeling of *E. coli* FrdAB catalytic voltammetry by Scheme 2, using the conditions given in Figure 13. Parameters: $K_M^{app} = 161\ \mu M$, $k_{cat} = 840\ s^{-1}$, $\Gamma = 2.93$ pmol cm^{-2}, $D = 1.24 \times 10^{-5}$ cm^2 s^{-1}, $\nu = 0.01$ cm^2 s^{-1}, $E_1 = -0.10$ V, $E_2 = 0$ V, $E_{C1} = -0.06$ V, $E_{C2} = -0.32$ V, $k_{C1O} = k_{C1H} = 1610\ s^{-1}$, $k_{C2O} = k_{C2H} = 238\ s^{-1}$, $k_2 = 9240\ s^{-1}$. The top graph shows the measured (symbols) and predicted (lines) limiting currents. The bottom graph shows the derivatives d*i*/d*E* of the predicted waves at 100, 200, 350, 500, 1000, and 3000 rpm.

with

$$k_{relay}^{max} = \left(\frac{1}{k_{C1O} + k_{C2O}} + \frac{1}{k_{C1H} + k_{C2H}}\right)^{-1} \qquad (21)$$

Finally, the value of G_{lim} is selected to predict the derivative peak potentials: the position of the low-potential wave is a particularly good indicator because the reduction potential of center 2 in the enzyme film is known with confidence (−320 mV at 25 °C, pH 7).[3]

The fit to the limiting current versus rotation rate yields $D = 1.2 \times 10^{-5}$ cm^2 s^{-1} and $\Gamma = 2.9$ pmol cm^{-2}. These values are similar to those reported previously ($D = 1.1 \times 10^{-5}$ cm^2 s^{-1} and $\Gamma = 3$ pmol cm^{-2}).[3,5] Good fits to the relative height of the low-potential wave versus rotation rate and fumarate concentration could be obtained for G_{lim} values up to at least 100, by adjusting k_{C2O}/k_{C1O} (yielding a higher k_{C2O}/k_{C1O} for higher G_{lim}). However, as the relay rates increase, the predicted derivative peaks move to higher potentials (see also Figure 10), and good agreement with the measured peak potentials is obtained only when $k_{relay}^{max} < k_2$. In this case the width of the low-potential wave 2 is predicted correctly ($n = 1.0$ under all conditions) and the amplitudes of wave 2 are as measured when $k_{C2O} < k_{C1O}$. Figure 14 shows the results obtained for $k_{relay}^{max} = k_2/10$ and $k_{C2O} = 0.15k_{C1O}$.

The main discrepancy between the model and the data is the shape of the first wave, which broadens and "tails" instead of being sharp as the model predicts. The trends of lower *n*-values with increasing rotation rate or fumarate concentration are very similar to the experimental data, but the best fits yield *n*-values that are too high by approximately 0.5. Predicted half-wave potentials for the first wave are only a few millivolts below the derivative peak potential, while the observed half-wave potentials may be at least 40 mV lower under conditions of high turnover, indicative of a very asymmetrical wave. This suggests that additional factors limit the electron-transfer rates, such as interfacial electron transfer to the iron−sulfur clusters, or slow electron transfer from center 3 to 1. The "tailing" may also be due to slow *direct* electron transfer to FAD, resulting in a low-amplitude third catalytic wave overlapping the first wave. Alternatively, the large observed asymmetry of the first wave can, at least partly, be explained by binding of substrate to the Ox and HalfRed states (including these equilibria results in an asymmetric wave, without changing the general properties of the model).

The calculations give the best agreement with the experimentally observed magnitudes and positions of both catalytic waves when electron relay via center 1 is rate-limiting and center 2 provides a boost to the total relay rate, but individual relay rates via center 2 are slower than those via center 1. However, this does not reveal which of the FAD reduction steps is rate-limiting (see Table 1). High scan rate cyclic voltammetry in the absence of fumarate showed that FAD reduction is mediated by one of the high-potential centers and is slower at high pH. This retardation coincides with both the lowering of the FAD reduction potential relative to centers 1 and 3 and the increase in magnitude of the second catalytic wave. Since the FAD is a cooperative two-electron couple ($E_1 < E_2$) with an average (two-electron) reduction potential close to that of center 1, the latter is a poor reductant for the first step (formation of the energetically unfavorable semiquinone radical) but a better reductant for the second flavin reduction step. The observations thus suggest that transfer of the *first* electron to FAD is rate-limiting.

Conclusions

A general steady-state model has been presented for a (sub)-monolayer of enzyme molecules adsorbed at a rotating disk electrode, catalyzing a two-electron substrate reduction. The model describes the influence of substrate mass transport, kinetic and redox properties of the active site, and electron-transfer limitations on the shape of catalytic waves. By use of the model of Scheme 1, a good approximation to the catalytic voltammograms of yeast cytochrome *c* peroxidase can be obtained. A subtle but reproducible feature of the wave shape is explainable in terms of turnover being limited by a chemical step during regeneration of resting [Fe(III)] enzyme from compound I. The extended model of Scheme 2, representing the simplest possible implementation of the dual relay mechanism proposed for *E. coli* fumarate reductase, reproduces most of the features of the catalytic waves when k_{cat} is limited by intramolecular electron relay. The ability to model complex experimental voltammetry data and thereby gain an alternative *potential-domain* description of kinetic patterns presents a compelling case for voltammetric methods in fundamental studies of catalytic electron transport in enzymes.

Acknowledgment. This work was supported by the Wellcome Trust (Grant 042109), and by the U.K. EPSRC. We thank Dr. Madhu S. Mondal and Ms. Kerensa Heffron for providing the C*c*P data and for helpful discussions.

Appendix A: Electron-Transfer Rates

For electron transfer from a solid electrode to an adsorbed species with reduction potential $E°$, Chidsey[23] derived a relation

between electron-transfer rate constants and overpotential by integrating the Marcus equation (A1), which describes the rate of electron transfer between a donor D and acceptor A over all Fermi levels E_i in the electrode, using the Fermi−Dirac distribution to account for the probability of occupancy of each level:

$$k_{ET}^{DA} = \frac{2\pi^2 V_0^{\,2} \exp(-\beta r)}{N_A h RT \sqrt{\pi \frac{F}{RT}\lambda}} \exp\left(-\left(\frac{F}{RT}(E_D - E_A + \lambda)\right)^2 / 4\frac{F}{RT}\lambda\right) \tag{A1}$$

In normalized form, this yields

$$\frac{k_{ET}(\Psi,\Lambda)}{k_{max}} = \frac{1}{\sqrt{4\pi\Lambda}} \int_{-\infty}^{\infty} \frac{\exp(-(\Lambda + \Psi - x)^2/4\Lambda)}{1 + \exp(x)}\, dx \tag{A2}$$

with $\Lambda = \lambda F/RT$, $\Psi = (E - E°)F/RT$, and $x = (E - E_i)F/RT$ where λ is the reorganization energy in electronvolts (the energy required to change the nuclear configuration of the reactant into that of the product ground state without electron transfer). The maximum electron-transfer rate constant at high overpotential is given by

$$k_{max} = k_{ET}(E \rightarrow -\infty) = \frac{4\pi^2 V_0^{\,2}}{N_A h RT} \exp(-\beta r) \tag{A3}$$

where V_0^2 is the maximum electronic coupling between donor and acceptor, r is the distance between donor and acceptor, and β describes the contribution made by the intervening medium in propagating the wave function. The integral is a sigmoidal function of potential. The rate constant is half its maximum value at $\Psi = -\Lambda$, i.e., where the overpotential equals the reorganization energy; thus the sigmoidal becomes less steep with increasing reorganization energy. The (calculated) rate constant at $\Psi = 0$ (i.e., the standard rate constant k_0) is proportional to k_{max} (at given λ), and decreases with increasing λ (at given k_{max}).

In voltammetric simulations, the integral function (eq A2) can be approximated numerically by summation over a sufficiently wide range of x:

$$\frac{k_{ET}(\Psi,\Lambda)}{k_{max}} \approx \frac{a}{s\sqrt{\pi}} \sum_{i=0}^{s} \frac{\exp(-(\Lambda + \Psi - x_i)^2/4\Lambda)}{1 + \exp(x_i)} \tag{A4}$$

with

$$x_i = x_p + a\left(\frac{2i}{s} - 1\right)\sqrt{\Lambda} \tag{A5}$$

and

$$x_p \approx \begin{cases} \Psi + \Lambda & \text{for} \quad \Psi \le -\Lambda - 5 \\ \Psi - \Lambda & \text{for} \quad \Psi \ge \Lambda + 5 \\ \dfrac{5\Psi}{\Lambda + 5} & \text{for} \quad -\Lambda - 5 < \Psi < \Lambda + 5 \end{cases} \tag{A6}$$

where the parameter a determines the range, s is the number of steps, and x_p is the "center of gravity" of the peak-shaped integrand (i.e., the x-value where the integrand is a maximum in the case of a symmetrical peak). With $a = 7$, $s = 100$, and $\Lambda < 100$, errors $\le 10^{-7}$ are obtained for all Ψ. With $\Psi = +(E - E°)F/RT$ the reduction rate constant k_{ET}^F is obtained, and with $\Psi = -(E - E°)F/RT$ the oxidation rate constant k_{ET}^B is obtained. The interfacial electron-transfer rate constants k_{E1}^F, k_{E1}^B, k_{E2}^F, and k_{E2}^B in the models are equal to k_{ET}^F and k_{ET}^B for $E^0 = E_1$ and $E^0 = E_2$, respectively.

Alternatively, the electron-transfer rates can be described by a semiempirical exponential dependence of the rate constants on overpotential according to the Butler−Volmer equation.[13] For reduction

$$k_{ET}^F = k_0 \exp\left(-\alpha \frac{nF}{RT}(E - E^0)\right) \tag{A7a}$$

while for oxidation

$$k_{ET}^B = k_0 \exp\left((1 - \alpha)\frac{nF}{RT}(E - E^0)\right) \tag{A7b}$$

Parameter α is the transfer coefficient, n is the number of electrons, and k_0 is the standard rate constant. For $\alpha = 0.5$, $n = 1$, and a given rate at zero overpotential k_0, the Butler−Volmer equation describes the limiting case of the integrated Marcus equation (eq A2) when the reorganization energy is infinitely high. Experimentally this implies that for a system with a reorganization energy much higher than the maximum applied overpotential (as is the case for many small molecules in water), the electron-transfer rates can usually be calculated with sufficient accuracy using the Butler−Volmer equation.

Appendix B: Steady-State Solution of Scheme 1

The steady-state differential equations for the enzyme species in the model are

$$\frac{\partial \Gamma_{Ox}}{\partial t} = 0 = -k_{E1}^F \Gamma_{Ox} + k_{E1}^B \Gamma_{HR} + k_2 \Gamma_{Red.S} \tag{B1a}$$

$$\frac{\partial \Gamma_{HR}}{\partial t} = 0 = k_{E1}^F \Gamma_{Ox} - (k_{E1}^B + k_{E2}^F)\Gamma_{HR} + k_{E2}^B \Gamma_{Red} \tag{B1b}$$

$$\frac{\partial \Gamma_{Red}}{\partial t} = 0 = k_{E2}^F \Gamma_{HR} - (k_{E2}^B + k_{+1}[S_{y=0}])\Gamma_{Red} + k_{-1}\Gamma_{Red.S} \tag{B1c}$$

$$\frac{\partial \Gamma_{Red.S}}{\partial t} = 0 = k_{+1}[S_{y=0}]\Gamma_{Red} - (k_{-1} + k_2)\Gamma_{Red.S} \tag{B1d}$$

where Γ_x is the surface coverage of species x and $[S_{y=0}]$ is the substrate concentration (by volume) at the electrode surface. With

$$\Gamma_{total} = \Gamma_{Ox} + \Gamma_{HR} + \Gamma_{Red} + \Gamma_{Red.S} \tag{B2}$$

the turnover number (rate per molecule) is given by

$$\text{turnover number} = k_2 \frac{\Gamma_{Red.S}}{\Gamma_{total}} = k_2 \Big/ \left(1 + \frac{\Gamma_{Red}}{\Gamma_{Red.S}}\left(1 + \frac{\Gamma_{HR}}{\Gamma_{Red}}\left(1 + \frac{\Gamma_{Ox}}{\Gamma_{HR}}\right)\right)\right) \tag{B3}$$

The concentration ratios can be found by rearrangement of the differential equations B1 (using K_M^∞, ϵ_1, and ϵ_2 as defined by

eqs 4b and 5b in the main text):

$$\frac{\Gamma_{Red}}{\Gamma_{Red.S}} = \frac{k_{-1} + k_2}{k_{+1}[S_{y=0}]} = \frac{K_M^\infty}{[S_{y=0}]} \quad \text{(B4a)}$$

$$\frac{\Gamma_{HR}}{\Gamma_{Red}} = \frac{k_{E2}^B}{k_{E2}^F} + \frac{k_{+1}[S_{y=0}]}{k_{E2}^F} - \frac{k_{-1}\Gamma_{Red.S}}{k_{E2}^F\,\Gamma_{Red}} = \epsilon_2 + \frac{k_2\,[S_{y=0}]}{k_{E2}^F\;K_M^\infty} \quad \text{(B4b)}$$

$$\frac{\Gamma_{Ox}}{\Gamma_{HR}} = \frac{k_{E1}^B}{k_{E1}^F} + \frac{k_2\,\Gamma_{Red.S}}{k_{E1}^F\;\Gamma_{HR}} = \epsilon_1 + \frac{k_2\,[S_{y=0}]\Gamma_{Red}}{k_{E1}^F\;K_M^\infty\;\Gamma_{HR}} \quad \text{(B4c)}$$

Substituting these solutions in eq B3 yields the turnover number as a function of the concentration of substrate close to the electrode surface and of applied potential:

$$\text{turnover number} = k_2/\left(1 + \frac{K_M^\infty}{[S_{y=0}]}\left(1 + \frac{\Gamma_{HR}}{\Gamma_{Red}}(1+\epsilon_1) + \frac{k_2\,[S_{y=0}]}{k_{E1}^F\;K_M^\infty}\right)\right) \quad \text{(B5)}$$

$$= k_2/\left(1 + (1 + \epsilon_2 + \epsilon_1\epsilon_2)\frac{K_M^\infty}{[S_{y=0}]} + k_2\left(\frac{1}{k_{E1}^F} + \frac{1+\epsilon_1}{k_{E2}^F}\right)\right)$$

Under steady-state conditions, the concentration of substrate at the surface is constant; thus the net transport of substrate from the bulk ($y \rightarrow \infty$) to the surface ($y = 0$) is equal to the turnover number:

$$\text{turnover number} = k_L([S_{bulk}] - [S_{y=0}]) \quad \text{(B6)}$$

Combining eqs B5 and B6, using the parameters H (potential dependence) and G (electron-transfer kinetics) as defined in the main text (eqs 5 and 6), and with $Q = [S_{y=0}]/[S_{bulk}]$, gives

$$k_L[S_{bulk}](1-Q)\left(1 + G + \frac{K_M^\infty/H}{Q[S_{bulk}]}\right) = k_2 \quad \text{(B7)}$$

and after rearrangement

$$Q^2 - PQ - \frac{K_M^\infty/H}{[S_{bulk}](1+G)} = 0 \quad \text{(B8)}$$

Parameter P is as defined in the main text (eq 7b). The roots of eq B8 are given by

$$Q = \frac{1}{2}\left(P \pm \sqrt{P^2 + \frac{4K_M^\infty/H}{[S_{bulk}](1+G)}}\right) \quad \text{(B9)}$$

Since no negative values of Q are allowed, the desired solution is as given in the main text (eq 7a).

Appendix C: Analysis of Steady-State Catalytic Wave Shapes

A symmetrical catalytic wave can be described by the Nernstian curve

$$i = \frac{i_{lim}}{1 + \exp\left(\frac{nF}{RT}(E - E_{1/2})\right)} \quad \text{(C1)}$$

where i_{lim} is the limiting (maximum) steady-state current for the catalytic wave (i.e., the current at low potential for a reduction) and $E_{1/2}$ is the half-wave potential (the potential where the current is half of i_{lim}). The apparent number of electrons, n, determines the steepness of the wave: a higher value of n results in a steeper wave, i.e., in a sigmoidal change from $i = 0$ to $i = i_{lim}$ that is more "compressed" around $E = E_{1/2}$.

The classical way to analyze a wave of this type is to plot ln $[(i_{lim} - i)/i]$ versus E (Heyrovský-Ilkovic′ plot[24]). For a symmetrical wave, this will give a straight line, zero at $E = E_{1/2}$ and with a slope of nF/RT. However, when multiple waves are present, i_{lim} has to be determined for each wave separately. In these cases, it is more convenient to analyze the derivatives di/dE. For a symmetrical wave, this yields a symmetrical peak around $E = E_{1/2}$, with a shape equal to that of a nonturnover peak for an adsorbed redox-active species. The n-value (also when apparent, noninteger) can therefore be derived from the peak width at half-height:

$$\delta = 3.53\frac{RT}{n_{app}F} \quad \text{(C2)}$$

Alternatively, n_{app} can be derived from the maximum slope of the wave (at $E = E_{1/2}$) as follows from eq C1 and its derivative:

$$n_{app} = -\frac{4RT}{Fi_{lim}}\left[\frac{di}{dE}\right]_{max} \quad \text{(C3)}$$

For FrdAB, the derivative peak is often "tailing" at low potential, and a second catalytic wave is present. Assuming that the second wave is symmetrical, the total current at low potential is given by

$$i_{total} = i_{tail}^1 + \frac{i_{lim} - i_{lim}^1}{1 + \exp\left(\frac{nF}{RT}(E - E_{1/2})\right)} \quad \text{(C4)}$$

where i_{tail}^1 and i_{lim}^1 are the estimated contributions of the first wave to the total current i_{total} and the limiting current i_{lim}, respectively. For the asymmetrical first wave, no theoretical shape is known. Therefore, we estimated the "tail" by extrapolation with a simple exponential decay function:

$$i_{tail}^1 = i_{lim}^1 + A(E - E_{lim})^B \quad \text{(C5a)}$$

for $E > E_{lim}$ and

$$i_{tail}^1 = i_{lim}^1 \quad \text{(C5b)}$$

for $E < E_{lim}$. E_{lim} is the potential at which i_{tail}^1 equals i_{lim}^1 and di_{tail}^1/dE is zero, and B determines the shape of the extrapolated tail. When a potential E^* is defined as the lowest potential where the contribution of the second peak still is negligible, the equation can be solved for given B, such that at $E = E^*$ the current i^* as well as its first and its second derivatives s^* and d^* are continuous:

$$i_{lim}^1 = i^* - A(E^* - E_{lim})^B \quad \text{(C6)}$$

$$A = \frac{s^*}{B(E^* - E_{lim})^{B-1}} \quad \text{(C7)}$$

and

$$E_{lim} = E^* - \frac{s^*}{d^*}(B - 1) \quad \text{(C8)}$$

Assuming that the second wave is symmetrical, its $E_{1/2}$ and n-value can be obtained from the wave ($i - i^1_{tail}$) and from the derivative peak d($i - i^1_{tail}$)/dE. The two waves can thus be separated by fitting the total current at $E < E^*$ to eq C4, with only E^* and B as variables.

References and Notes

(1) Sucheta, A.; Ackrell, B. A. C.; Cochran, B.; Armstrong, F. A. *Nature* **1992**, *356*, 361. Hirst, J.; Sucheta, A.; Ackrell, B. A. C.; Armstrong, F. A. *J. Am. Chem. Soc*. **1996**, *118*, 5031. Hirst, J.; Ackrell, B. A. C.; Armstrong, F. A. *J. Am. Chem. Soc*. **1996**, *119*, 7434.

(2) Moser, C. C.; Keske, J. M.; Warncke, K.; Farid, R. S.; Dutton, P. L. *Nature* **1992**, *355*, 796. Beratan, D. N.; Betts, J. N.; Onuchic, J. N. *Science* **1991**, *252*, 1285. *Protein Electron Transfer*; Bendall, D. S., Ed.; Bios Scientific Publishers: Oxford, England, 1996. Christensen, H. E. M.; Coutinho, I.; Conrad, L. S.; Hammerstad-Pedersen, J. M.; Iversen, G.; Jensen, M. H.; Karlsson, J. J.; Ulstrup, J.; Xavier, A. V. *J. Photochem. Photobiol. A: Chem.* **1994**, *82*, 103. See also Heller, A. *Acc. Chem. Res.* **1990**, *23*, 128, for an account of artificial "wiring" of enzymes.

(3) Heering, H. A.; Weiner, J. H.; Armstrong, F. A. *J. Am. Chem. Soc*. **1997**, *119*, 11628.

(4) Armstrong, F. A.; Heering, H. A.; Hirst, J. *Chem. Soc. Rev*. **1997**, *26*, 169.

(5) Sucheta, A.; Cammack, R.; Weiner, J.; Armstrong, F. A. *Biochemistry* **1993**, *32*, 5455.

(6) Xie, Y.; Anson, F. C. *J. Electroanal. Chem.* **1995**, *384*, 145. Xie, Y.; Anson, F. C. *J. Electroanal. Chem.* **1995**, *396*, 441. Xie, Y.; Anson, F. C. *J. Electroanal. Chem.* **1996**, *404*, 209. Bourdillon, C.; Demaille, C.; Moiroux, J.; Savéant, J. M. *J. Am. Chem. Soc.* **1995**, *117*, 11499. Bourdillon, C.; Demaille, C.; Moiroux, J.; Savéant, J. M. *Acc. Chem. Res.* **1996**, *29*, 529. Fang, H.; Chen, H. Y. *J. Electroanal. Chem*. **1997**, *432*, 171. Aoki, K.; Tokuda, K.; Matsuda, H. *J. Electroanal. Chem.* **1986**, *199*, 69. Andrieux, C. P.; Dumas-Bouchiat, J. M.; Savéant, J. M. *J. Electroanal. Chem.* **1981**, *123*, 171. Mell, L. D.; Maloy, J. T. *Anal. Chem.* **1975**, *47*, 299. Shu, F. R.; Wilson, G. S. *Anal. Chem.* **1976**, *48*, 1679. Kamin, R. A.; Wilson, G. S. *Anal. Chem.* **1980**, *52*, 1198.

(7) Andrieux, C. P.; Savéant, J. M. *J. Electroanal. Chem.* **1982**, *134*, 163. Xie, Y.; Anson, F. C. *J. Electroanal. Chem.* **1993**, *344*, 405. Sabatani, E.; Anson, F. C. *J. Phys. Chem.* **1993**, *97*, 10158.

(8) Laviron, E. In *Electroanalytical Chemistry*; Bard, A. J., Ed.; Marcel Dekker: New York, 1982; Vol. 12, pp 53−157.

(9) The principles and experimental demonstrations of mass transport to microelectrode array electrodes are described in several publications. See, for example, Sabatini, E.; Rubinstein, I. *J. Phys. Chem.* **1987**, *91*, 6663; Bard, A. J.; Crayston, J. A.; Kittlesen, G. P.; Shea, T. V.; Wrighton, M. S. *Anal. Chem.* **1986,** *58*, 2321; Penner, R. M.; Martin, C. R. *Anal. Chem.* **1987,** *59*, 2625.

(10) The microelectrode array model for noncatalytic protein voltammetry is described in Armstrong, F. A.; Bond, A. M.; Hill, H. A. O.; Psalti, I. S. M.; Zoski, C. G. *J. Phys. Chem.* **1989**, *93*, 6485.

(11) Plichon, V.; Laviron, E. *J. Electroanal. Chem.* **1976**, *71*, 143.

(12) Niemz, A.; Imbriglio, J.; Rotello, M. *J. Am. Chem. Soc.* **1997**, *119*, 887. Zusman, L. D.; Beratan, D. N. *J. Phys. Chem. A* **1997**, *101*, 4136.

(13) Bard, A. J.; Faulkner, L. R. *Electrochemical Methods, Fundamentals and Applications*; Wiley: New York, 1980.

(14) Consequently, Koutecky−Levich analysis of experimental data may not yield correct values of K_M, k_{cat}, and the diffusion coefficient. Although the Koutecky−Levich plots are linear at low rotation rates (with a slope as predicted from the diffusion coefficient), $1/i_{lim}$ becomes independent of $1/\omega^{1/2}$ at high rotation rates. This results in overestimation of the substrate diffusion coefficient (D) and yields intercepts below the modelled $1/i_{lim}$ at $\omega \rightarrow \infty$, particularly at higher [S] or lower $k_2\Gamma$. Thus a plot of the intercepts $1/i_{lim}$ versus 1/[S] may significantly deviate from the Lineweaver−Burk plot expected for the given k_2 and K_M^∞ when $L < 0.1$ at the lowest rotation rates. For [S] < K_M^∞ the intercepts follow a trend parallel to the expected plot, while for [S] > K_M^∞ the intercepts become less dependent on [S] and even increase for very large [S]. For example, using substrate concentrations between 0.3 and 3 times K_M^∞ and rotation rates rates between 100 and 3000 rpm, Koutecky−Levich analysis yields approximately correct values of k_2 and K_M^∞ but overestimates D when $k_2\Gamma < 1$ nmol cm^{-2} s^{-1} ($L > 0.1$). However, for experiments subject to greater mass-transport control (higher $k_2\Gamma$), it tends to overestimate both k_2 and K_M^∞ while giving an approximately correct diffusion coefficient.

(15) Coulson, A. J. W.; Erman, J. E.; Yonetani, T. *J. Biol. Chem.* **1971**, *246*, 917.

(16) Liu, R.-Q.; Miller, M. A.; Han, G. W.; Hahm, S.; Geren, L.; Hibdon, S.; Kraut, J.; Durham, B.; Millett, F. *Biochemistry* **1994**, *33*, 8678.

(17) Mondal, M. S.; Fuller, H. A.; Armstrong, F. A. *J. Am. Chem. Soc*. **1996**, *118*, 263: Mondal, M. S.; Goodin, D. B.; Armstrong, F. A. *J. Am. Chem. Soc*. **1998**, *120*, 6270−6276.

(18) Lannon, A. M.; Armstrong, F. A. *J. Am. Chem. Soc*. **1987,** *109*, 7211. Paddock, R. M.; Bowden, E. F. *J. Electroanal. Chem*. **1989**, *260*, 487. Scott, D. L.; Paddock, R. M.; Bowden, E. F. *J. Electroanal. Chem.* **1992**, *341*, 307. Armstrong, F. A.; Bond, A. M.; Buchi, F.; Hamnett, A.; Hill, H. A. O.; Lannon, A. M.; Lettington, O. C.; Zoski, C. G. *Analyst* **1993**, *118*, 973.

(19) A manuscript presenting the analysis of C*c*P nonturnover signals and catalytic waves is in preparation. A value for k_0 of approximately 6 s^{-1} is obtained by analyzing the shape and position of the nonturnover peaks at increasing scan rates or by using potential step voltammetry.

(20) Balny, C.; Anni, H.; Yonetani, T. *FEBS Lett.* **1987**, *221*, 349. Goodin, D. B.; Davidson, M. G.; Roe, J. A.; Mauk, G.; Smith, M. *Biochemistry* **1991**, *30*, 4953. Vitello, L. B.; Erman, J. E.; Miller, M. A.; Wang, J.; Kraut, J. *Biochemistry* **1993**, *32*, 9807.

(21) (a) Reference 16 suggests that a rate-determining conversion from the [Fe(IV):Trp^0] form of compound II to the [Fe(III):Trp$^{\bullet +}$] form occurs before reduction to the resting enzyme. (b) It has been reported that oxidation of horseradish peroxidase by [Ru(2,2′-bipyridine)$_3$]$^{3+}$ initially generates an Fe(III) π-cation porphyrin radical intermediate, followed by a rate-limiting conversion to the Fe(IV) form of compound II and fast further oxidation to produce compound I (Berglund, J.; Pascher, T.; Winkler, J. R.; Gray, H. B. *J. Am. Chem. Soc*. **1997**, *119*, 2464).

(22) Hahn, S.; Geren, L.; Durham, B.; Millett, F. *J. Am. Chem. Soc.* **1993**, *115*, 3372.

(23) Chidsey, C. E. D. *Science* **1991**, *251*, 919.

(24) Bond, A. M. *Modern polarographic methods in analytical chemistry*; Dekker: New York, 1980.